Hindawi
Shock and Vibration
Volume 2019, Article ID 2854836, 14 pages
https://doi.org/10.1155/2019/2854836

Research Article

A Fuzzy-Based Analytic Hierarchy Process for Mechanical Noise Source Identification of a Diesel Engine

Junhong Zhang,[1,2] Qidi Zhou ,[1] Jiewei Lin ,[1] Weidong Li,[1] Zhoujie Tang,[1] and Chaoyang Duan[1]

[1]*State Key Laboratory of Engines, Tianjin University, Tianjin 300072, China*
[2]*Renai College, Tianjin University, Tianjin 301636, China*

Correspondence should be addressed to Jiewei Lin; linjiewei@tju.edu.cn

Received 23 June 2018; Revised 19 November 2018; Accepted 14 January 2019; Published 10 February 2019

Academic Editor: Andrea Spaggiari

Copyright © 2019 Junhong Zhang et al. This is an open access article distributed under the Creative Commons Attribution License, which permits unrestricted use, distribution, and reproduction in any medium, provided the original work is properly cited.

In this paper, a novel fuzzy-based analytic hierarchy process (FAHP) is proposed for identifying noise sources of diesel engine and sorting their contributions. The hierarchy tree consists of 5 levels including the component level, the frequency band level, the test point level, the operating condition level, and the overall noise level. The variational mode decomposition (VMD) is employed to decompose the overall noise into several frequency bands. The factor weights between levels are determined by the partial coherence analysis (PCA) to consider the correlation of component vibration and radiated noise in different frequency bands. A fuzzy consistency matrix is then constructed to order the corresponding factors level by level that can avoid the consistence problem of the traditional AHP. Based on the rig test of a diesel engine, the proposed approach is implemented to weight the noise sources identified. It is shown the overall weighting order of the six major noise sources is (in descending order) the oil pan, the left block, the valve cover, the flywheel housing, and the right block.

1. Introduction

NVH problems are increasingly important in nowadays automobile industry, and reduction in engine noise is one of the most concerns. A precise recognition of the noise sources and their contribution is the first step in interior noise control [1–3].

In the noise source identification of the engine, signal processing-based approach is quite popular these days because of its comprehensive performance in accuracy [4, 5], flexibility, and cost-saving [6, 7]. Lots of method have been proposed, such as the cyclic Wiener filtering [8, 9], the time-frequency analysis [10–12], the blind source separation [13, 14], and the coherent spectrum analysis (CSA) [15]. But it is still very difficult for only using one signal processing method to perfectly handle the complex noise problem. For this reason, the analytic hierarchy process (AHP) [16, 17] has been proved suitable for decision-making of complex systems. It has been widely used in social, political, economic, and technological problems with multiple choices. In the noise identification of the diesel engine, a great amount of factors should be considered, such as frequency, engine speed, load, and component. Besides, correlations between factors (e.g., frequency band and component vibration and vibration between component and radiated noise) have influence on the weighting coefficients of the noise source. In this situation, the AHP could be an effective solution in weighting noise sources of a diesel engine. Liang [18] utilized the cepstrum analysis and the AHP in weighting the noise contribution from engine components. The overall noise was decomposed into five frequency bands, and one operating speed was considered. Zhang et al. [19] proposed a combined AHP approach to analyse the contribution of different engine parts to the overall radiated noise in different engine speeds. The decomposition by ensemble empirical mode decomposition (EEMD) was affected by the modal aliasing problem in intrinsic mode functions (IMFs). And the coherent spectrum analysis (CSA) is limited in the case that multiple inputs are not independent from each other.

On the contrary, some limits have been found for the traditional AHP approach [20, 21]: (1) the consistency of the judgment matrix is very costly to achieve, (2) preferences mismatch the objective priority, and (3) the uncertainty of

subjective evaluation reduces the accuracy. To overcome the above shortages, the fuzzy-based AHP (FAHP) [22, 23] is developed to take into account the uncertainty in decision-making. A fuzzy scale is used to express the preference or relative importance of the target property instead of adopting an exact value from pairwise comparison. In addition, the fuzzy consistency matrix [24–27] used in the FAHP can be determined by membership functions (MFs), so the consistency of the judgment matrix is met automatically [28, 29]. It can be seen that the FAHP is able to improve the traditional noise source weighting approach as long as reasonable structures and components of the hierarchy tree is built.

In this paper, a novel approach based on the FAHP is proposed to weight the noise sources of the diesel engine. Based on a rig test, the overall noise is decomposed into several frequency bands using the variational mode decomposition (VMD). Then, the correlation between the vibration of engine component and the overall radiated noise is analysed through partial coherence analysis (PCA). A FAHP is constructed to determine the weights of the component to the overall noise. Finally, the identification results are verified by the near-field noise measurement.

2. Methods

2.1. Variational Mode Decomposition. The VMD algorithm [30] is a self-adaptive signal processing method, which can decompose a mixed signal into a number of IMFs. The discrete subsignals have finite orders of mode with specific sparsity properties for being reconstructed back to the original signal [31]. The constrained variational problem is given as follows:

$$\begin{aligned} &\min_{\{\mu_k\},\{w_k\}} \left\{ \sum_k \left\| \partial_t \left[\left(\partial(t) + \frac{j}{\pi t} \right) \mu_k(t) \right] e^{-jw_k t} \right\|_2^2 \right\}, \\ &\text{s.t.} \quad \sum_k \mu_k = f, \end{aligned} \tag{1}$$

where $\{\mu_k\} = \{\mu_1, \ldots, \mu_k\}$ and $\{\omega_k\} = \{\omega_1, \ldots, \omega_k\}$ are the modal components and the corresponding centre frequencies, $\sum_k = \sum_{k=1}^{K}$ is the summation of modes, k is the number of modes, and f is the input signal. To make the problem unconstraint, it is necessary to bring in the quadratic penalty factor α and the Lagrange multiplier λ. The quadratic penalty factor is used to improve the high reconstruction accuracy in dealing with the Gaussian noise. The Lagrange multiplier can enforce constraints effectively, which can be obtained as follows:

$$\begin{aligned} L(\{\mu_k\}, \{\omega_k\}, \lambda) = \alpha \sum_k \left\| \partial_t \left[\left(\delta(t) + \frac{j}{\pi t} \right) \mu_k(t) \right] e^{-j\omega_k t} \right\|_2^2 \\ + \left\| x(t) - \sum_k \mu_k(t) \right\|_2^2 + \langle \lambda(t), f(t) - \sum_k \mu_k(t) \rangle. \end{aligned} \tag{2}$$

Using the alternate direction method of multipliers for the extended Lagrange expression through alternating optimization of μ_k, ω_k, and λ, the optimal solution of the equation can be obtained. The VMD method can be implemented by the following steps:

Step 1. Initialize $\{\mu_k^1\}$, $\{\omega_k^1\}$, and λ^1, and set $n = 0$.

Step 2. Count $n = n + 1$.

Step 3. For $k = 1:1:k$, obtain

$$\begin{aligned} \mu_k^{n+1} &= \arg\min_{\mu_k} L\left(\left\{ \mu_{i<k}^{n+1} \right\}, \left\{ \mu_{i\geq k}^{n} \right\}, \left\{ \omega_i^n \right\}, \lambda^n \right), \\ \omega_k^{n+1} &= \arg\min_{\omega_k} L\left(\left\{ \mu_i^{n+1} \right\}, \left\{ \mu_{i<k}^{n+1} \right\}, \left\{ \omega_{i\geq k}^{n} \right\}, \lambda^n \right), \\ \lambda^{n+1} &= \lambda^n + \tau \left(f - \sum_k \mu_k^{n+1} \right). \end{aligned} \tag{3}$$

Step 4. Judge the convergence:

$$\sum_k \frac{\left\| \mu_k^{n+1} - \mu_k^n \right\|_2^2}{\left\| \mu_k^n \right\|_2^2} < c, \tag{4}$$

where c is the convergence judgment condition. The program stops if the convergence is met at Step 4; otherwise, the iteration circulates from Steps 2 to 4.

A simulation signal $S = S_1 + S_2 + S_3 + S_4$ is given by the following equation:

$$\begin{aligned} S_1 &= 0.5\cos(2\pi \cdot 6t), \\ S_2 &= \cos(2\pi \cdot 20t), \\ S_3 &= \cos(2\pi \cdot 50t), \\ S_4 &= 0.3\cos(2\pi \cdot 400 \cdot t) e^{-10^4 \times (t-0.2)^2} \\ &\quad + 0.4\cos(2\pi \cdot 400t) e^{-10^4 \times (t-0.5)^2} \\ &\quad + 0.3\cos(2\pi \cdot 400t) e^{-10^4 \times (t-0.8)^2}. \end{aligned} \tag{5}$$

Figure 1 shows the original components of S_1 to S_4 and the decomposed IMFs by VMD. It can be seen clearly that the simulation signal S is accurately decomposed into four IMFs and the IMFs represent the characters of original components exactly.

2.2. Partial Coherence Analysis. For a multi-input single-output system with independent inputs, CSA is capable to estimate the relationship between input and output efficiently [32] while it is not the case in this paper. For engine noise, acoustic sources are correlated. It is not very appropriate to use CSA because wrong correlation between the radiated noise and the component vibration may be brought in. To avoid this, the PCA is applied because it can remove the coherence of other inputs from the target. So, the correlations between inputs and outputs can be found out properly as shown in Figure 2, and six input channels represent the main acoustic sources of mechanical noise including the oil pan (X_1), the left block (X_2), the right block (X_3), the gear cover (X_4), the flywheel housing (X_5), and the valve cover (X_6). L_1 to L_6 are the conditioned transfer

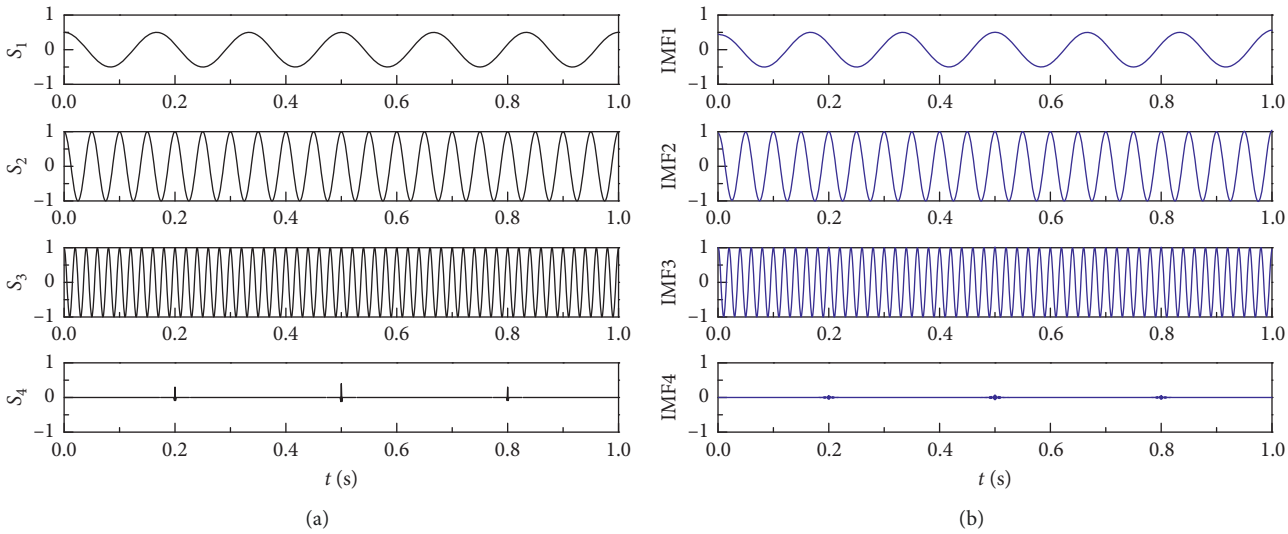

Figure 1: Components from (a) original signal and (b) decomposition of VMD.

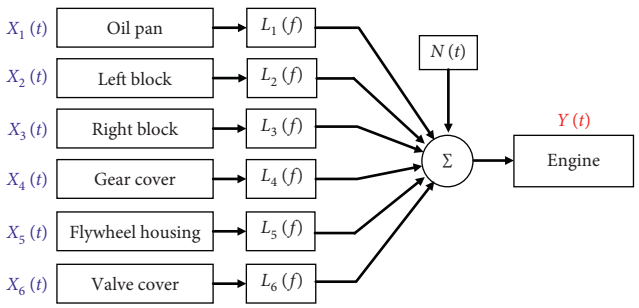

Figure 2: The PCA diagram in engine noise identification.

functions of corresponding acoustic source, where $N(t)$ is the sensor noise, $Y(t)$ is the IMFs of the measured acoustic signal.

The PCA can be adopted by the following steps [33]:

Step 1. Transform signals from time domain into frequency domain, $X(t), Y(t) \longrightarrow X(f), Y(f)$.

Step 2. Calculate the self-power spectra and the cross-power spectra of the transformed signals:

$$S_{xx} = \frac{1}{MN_{\mathrm{FFT}}} \sum_{i=1}^{M} X_i(f) X_i^*(f),$$

$$S_{yy} = \frac{1}{MN_{\mathrm{FFT}}} \sum_{i=1}^{M} Y_i(f) Y_i^*(f), \tag{6}$$

$$S_{xy} = \frac{1}{MN_{\mathrm{FFT}}} \sum_{i=1}^{M} X_i(f) Y_i^*(f),$$

where S_{xx} and S_{yy} represent the self-power spectra of the input and the output respectively, S_{xy} represents the cross-power spectrum of the input and output, and $X_i^*(f)$ and $X_i^*(f)$ are conjugate complex numbers of $X_i(f)$ and $Y_i(f)$.

Step 3. Calculate the conditioned transfer functions and the conditioned power spectra:

$$L_{ij} = \frac{S_{ij\cdot(i-1)!}}{S_{ii\cdot(i-1)!}},$$

$$S_{ij\cdot r!} = S_{ij\cdot(r-1)!} - L_{rj} S_{ir\cdot(r-1)!}, \tag{7}$$

$$S_{jj\cdot r!} = S_{jj\cdot(r-1)!} - L_{rj} S_{jr\cdot(r-1)!},$$

where L_{ij} is the conditioned transfer function, $S_{ij\cdot r!}$ is the conditioned cross-power spectrum between the input and output without coherent effects from $X_1, X_2, \ldots, X_r$, and $S_{jj\cdot r!}$ is the conditioned self-power spectrum without coherent effects from other signals.

Step 4. Calculate the input partial coherent power spectrum:

$$\gamma_{iy\cdot r!}^2 = \frac{\left|S_{iy\cdot r!}\right|^2}{S_{ii\cdot r!} S_{yy\cdot r!}}, \tag{8}$$

$$S'_{yxi} = \gamma_{iy\cdot r!}^2 S_{ii\cdot r!},$$

where $\gamma_{iy\cdot r!}^2$ is the partial coherent function describing the correlation between $X_i(t)$ and $Y(t)$ in the whole frequency range, $S_{ii\cdot r!}$ is the conditioned self-power spectrum, and S'_{yxi} is the input partial coherent power spectrum (PCPS) that shows the relationship between component vibration and radiated noise.

2.3. Fuzzy AHP. The detailed process of the FAHP can be described as follows:

Step 1. Establish the fuzzy judgment matrix $\mathbf{A}$ from pairwise comparisons. Determine the fuzzy judgment matrix $\mathbf{A} = [a_{ij}]_{n\times n}$ according to the relative importance of factors in the same layer. The elements in matrix $\mathbf{A}$ are in the range of 0.1 to 0.9, where 0.5 represents the two factors are equally important.

Step 2. Calculate the fuzzy consistency matrix **R** and the reciprocal matrix **M**. Transform $\mathbf{A} = [a_{ij}]_{n\times n}$ into $\mathbf{R} = [r_{ij}]_{n\times n}$. The calculation can be done by the following equation:

$$r_{ij} = \frac{1}{2n}\left(\sum_{k=1}^{n} a_{ik} - \sum_{k=1}^{n} a_{jk}\right) + 0.5. \tag{9}$$

Then, the matrix **R** can be converted into the reciprocal fuzzy consistency matrix **M** through $m_{ij} = r_{ij}/r_{ji}$.

Step 3. Calculate the initial weighting vector ω_0. The initial weighting vector $\omega_0 = [\ \omega_1\ \ \omega_2\ \cdots\ \omega_n\ ]$ can be obtained by the least-squares method:

$$\begin{cases} \omega_0 = \dfrac{1}{n} - \dfrac{1}{2\partial} + \dfrac{1}{n\partial}\displaystyle\sum_{j=1}^{n} r_{ij}, \\ \\ \partial = \dfrac{n-1}{2}. \end{cases} \tag{10}$$

Step 4. Calculate the final weighting vector **V**:

(1) Initialize $V_0 = [\ v_{0,1}\ \ v_{0,2}\ \cdots\ v_{0,n}\ ]$ by ω_0

(2) For $k = 1, 2, 3, \ldots, n$,

$$V_{k+1} = MV_k. \tag{11}$$

(3) Check the convergence by the following equation:

$$\|V_{k+1}\|_{\infty} - \|V_k\|_{\infty} \le \varepsilon. \tag{12}$$

(4) If the convergence is met, output the final weighting vector as follows:

$$V_{k+1} = \left[\ \frac{V_{k+1,1}}{\sum_{i=1}^{n} V_{k+1,i}}\ \ \frac{V_{k+1,2}}{\sum_{i=1}^{n} V_{k+1,i}}\ \ \frac{V_{k+1,3}}{\sum_{i=1}^{n} V_{k+1,i}}\ \cdots\ \frac{V_{k+1,n}}{\sum_{i=1}^{n} V_{k+1,i}}\ \right]. \tag{13}$$

Otherwise, jump back to Step 2.

2.4. Flow Chart. The overall framework is given in Figure 3, and the process can be divided into six steps:

Step 1. Decompose the noise signal into a series of IMFs in consecutive frequency bands by VMD.

Step 2. Analyse the relationship between component vibration and radiated noise through PCA to obtain the weighting order of components in each frequency band.

Step 3. Construct the hierarchy tree and establish the fuzzy consistency matrices. Obtain the contributions of noise sources to the decomposed noise in different frequency bands.

Step 4. Calculate the contributions of noise in different frequency bands to different test points according to the A-weighted SPL and construct the combined weight matrix of the test point level.

Step 5. Obtain the contributions of noise at different test points to different engine speeds and construct the combined weight matrix of the operating speed level.

Step 6. Construct the fuzzy consistency matrix of the objective level according to the A-weighted SPL and the usage rate of engine speeds and obtain the overall weights of noise sources.

3. Measurements

The noise and vibration experiment is carried out on a test rig in a semianechoic chamber with less than 18 dB background SPL, as shown in Figure 4. Acoustic signals are collected using five MA231 acoustic sensors (BSWA Technology Co. Ltd, China) 1 m away from the front, the rear, the left, the right, and the top surfaces of engine. The near-field noise (0.01 m away from the measuring surface) as well as the vibration of some highly concerned components is measured including the oil pan, the block, the flywheel housing, and the valve cover. In the vibration measurement, the triaxial accelerometers (PCB Piezotronics, Inc., US) are arranged at different regions for large component and the mean acceleration is employed. In order to reduce uncertainty error during the test, all the microphones and accelerometers are calibrated before the measurement according to the instructions in the test environment, and all the test cases are recorded for three times separately.

The experiment is carried out at four typical engine speeds of 700 r/min (idle), 1400 r/min (maximum torque), 1800 r/min (most commonly used operating condition of construction machinery with 80% load), and 2200 r/min (rated). The combustion settings of the four typical operating conditions are listed in Table 1. The sampling frequency is 10240 Hz, and the intake noise, the exhaust noise, and the fan noise are removed from the measurement.

4. Results and Discussion

In this section, only the 1800 r/min case is used as an example to show the results due to the huge amount of data, and the analysis procedure of other operating conditions is in the same way as the showcase.

4.1. Noise Decomposition. In order to improve signal decomposition accuracy, the trend term and cumulative error are eliminated from the raw data before the formal analysis. The central frequency of IMF is used as the criteria for choosing the best modal number K. Overdecomposition occurs when the difference of the central frequencies of two adjacent IMFs is smaller than 10% of the whole frequency range. Four K values are employed in this study including 4, 5, 6, and 7. The central frequencies of the corresponding IMFs are listed in Table 2. For $K = 7$, the central frequency difference of IMF4 and IMF5 is 147 Hz < 10% × whole frequency range (2707–240) = 246.7 Hz. As a result, the $K = 7$ case is considered as overdecomposition so that $K = 6$ is

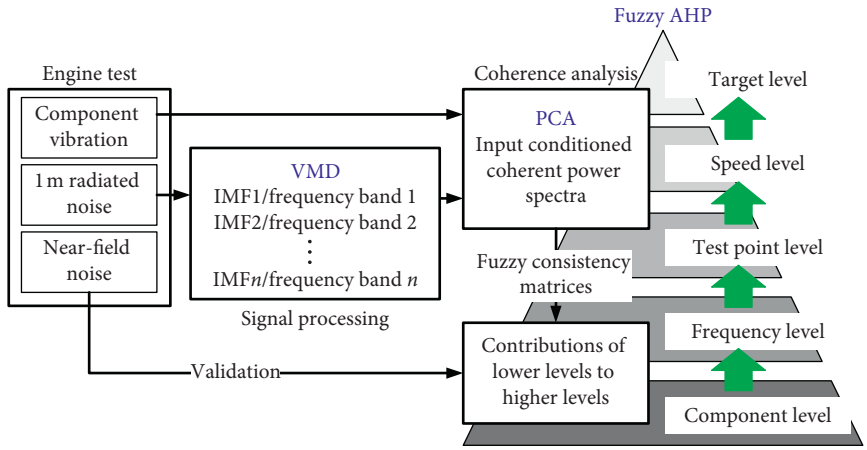

Figure 3: The overall framework of the noise source weighting process.

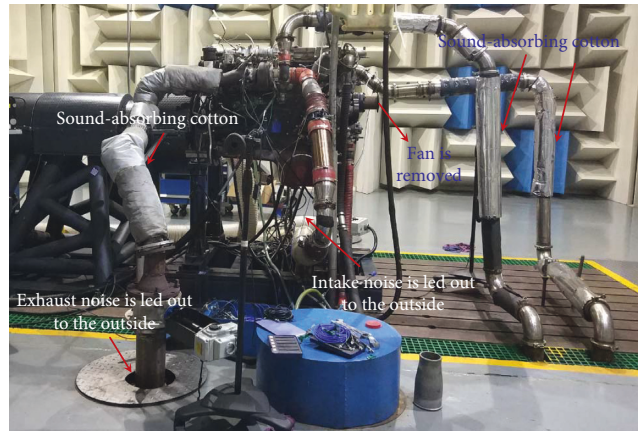

Figure 4: Arrangement of the noise and vibration test.

Table 1: The combustion settings of the four typical operating conditions.

Operating conditions	Intake pressure (MPa)	Intake temperature (°C)	Fuel injection timing (°CA)	Maximum in-cylinder pressure (MPa)	Fuel injection pressure (MPa)
Idle condition	0.0027	26	6.9	13.1	43.370
1400 r/min + 100% load	0.2497	51	4.1	18.4	154.478
1800 r/min + 80% load	0.1879	48.4	10.8	18.1	178.243
Rated condition	0.1749	48.3	11.2	17.9	179.441

employed in the VMD decomposition. The IMFs obtained from the acoustic signal recorded at the left-side test point at 1800 r/min are given in Figure 5.

The lower and upper limits of the frequency band are determined by time-frequency analysis using wavelet transform. As shown in Figure 6, the six frequency bands are 0–500 Hz, 500–800 Hz, 800–1200 Hz, 1200–1800 Hz, 1800–2500 Hz, and 2500–4000 Hz. In lower frequency ranges, e.g., 0–500 Hz and 500–800 Hz, obvious periodicity can be found for the radiated noise. This periodic character corresponds to the ignitions of cylinder. The six consecutive highlight parts along the time correlate to the ignitions of the six cylinders in a working cycle (720°CA in 0.4 s at 1800 r/min). Most engine parts contribute to the low frequency radiated noise because their lower vibration modes fall in these frequency bands. For higher frequency, the energy distribution still shows periodic characters but more details within every single stroke can be found. From this point of view, each IMF has its own physical meaning, and it can improve the reliability of the following PCA.

Table 2: Decomposition results with different modal numbers.

Modal number K	Central frequencies (Hz)						
	IMF1	IMF2	IMF3	IMF4	IMF5	IMF6	IMF7
4	276	766	1442	2596	—	—	—
5	274	762	1384	1780	2675	—	—
6	251	577	823	1409	1924	2702	—
7	240	561	810	1245	1392	1922	2707

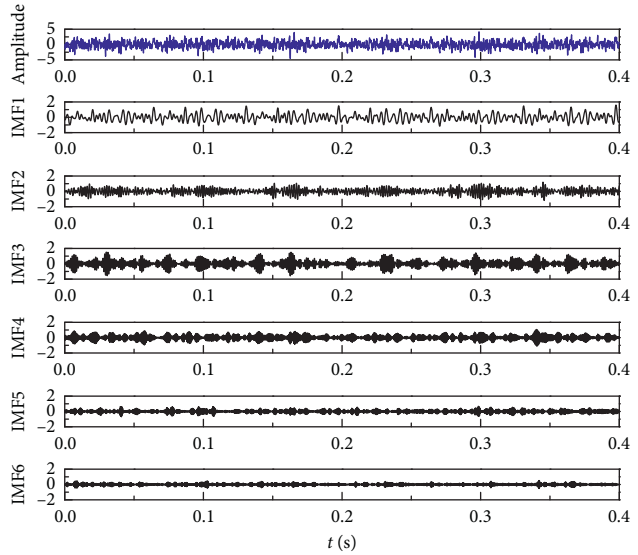

Figure 5: The measured and VMD decomposed signals from the left-side test point at 1800 r/min.

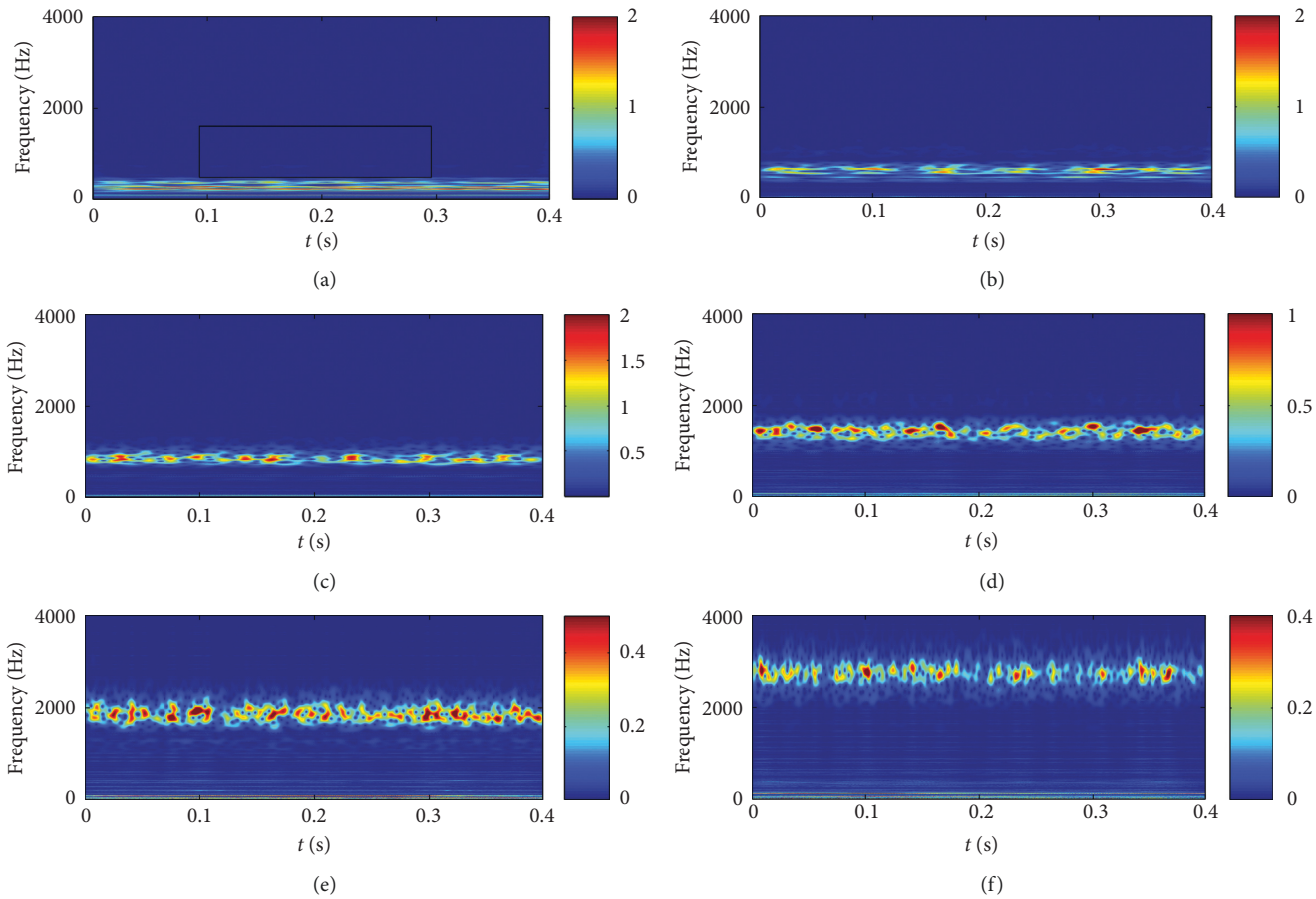

Figure 6: Time-frequency results of IMFs.

4.2. Partial Coherence Analysis. The radiated noise of the engine contains the vibration information of the engine component, so the contributions of various components to the measured noise can be identified according to the correlation between noise and vibration. Many of the accessories are rigidly connected to the engine block, so the vibration between different noise sources is coupled. It is why the PCA is chosen to recognize the correlation of component vibration and radiated noise. The input partial coherent power spectra (PCPS) of the 1800 r/min case are shown in Figure 7.

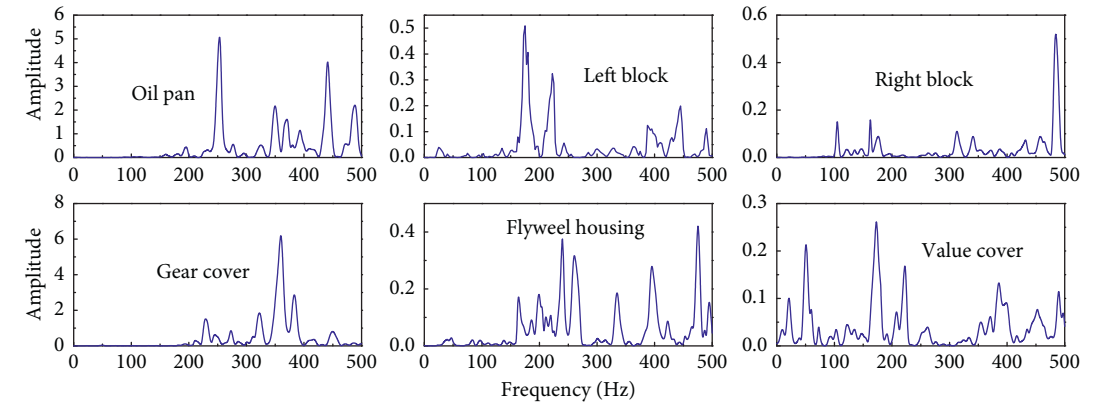

(a)

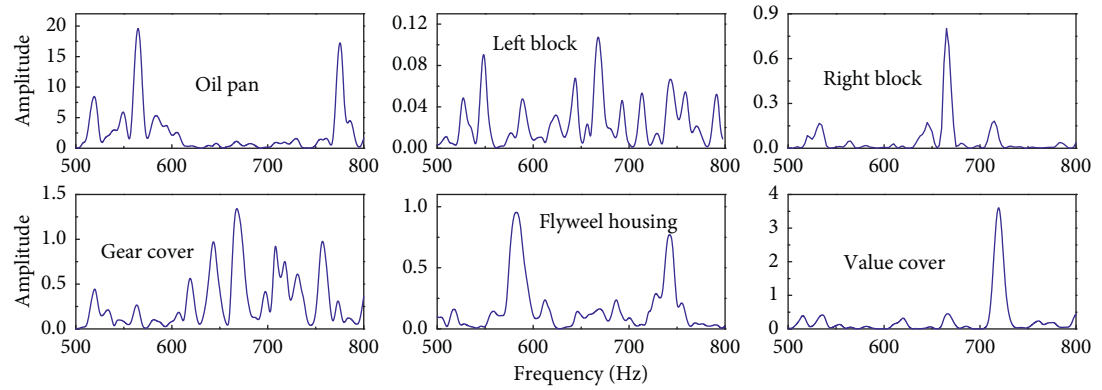

(b)

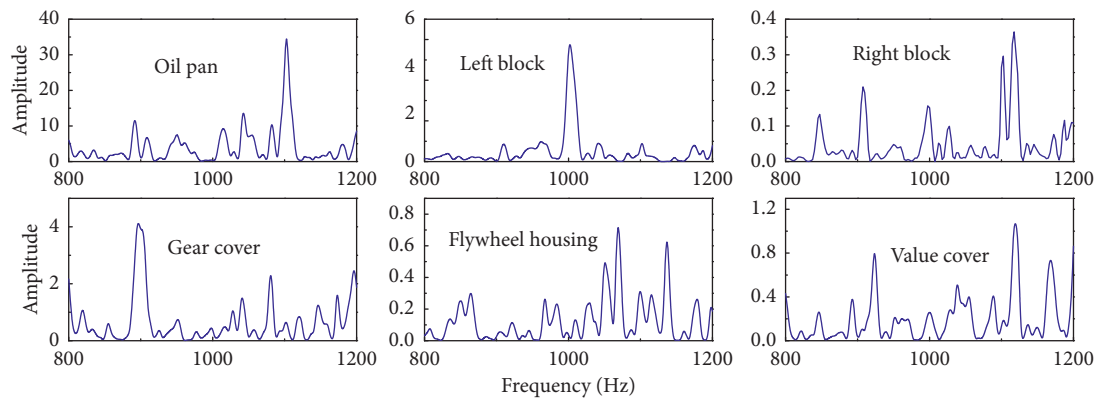

(c)

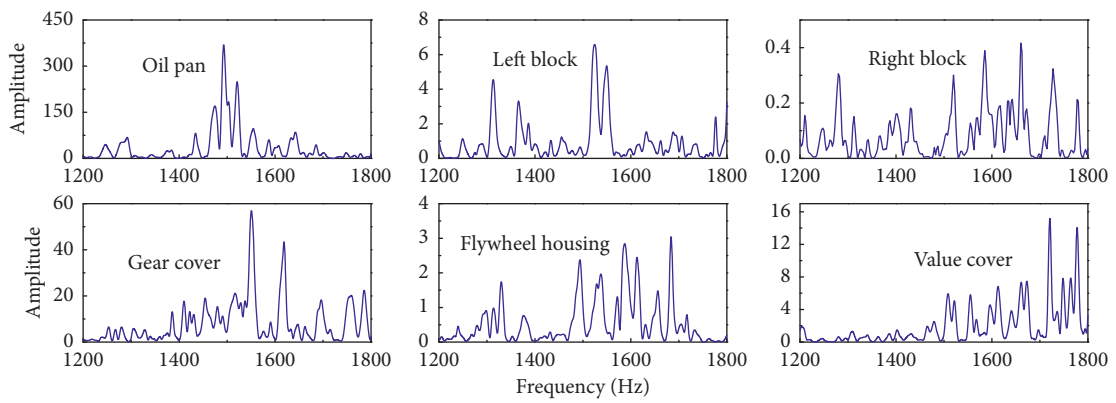

(d)

Figure 7: Continued.

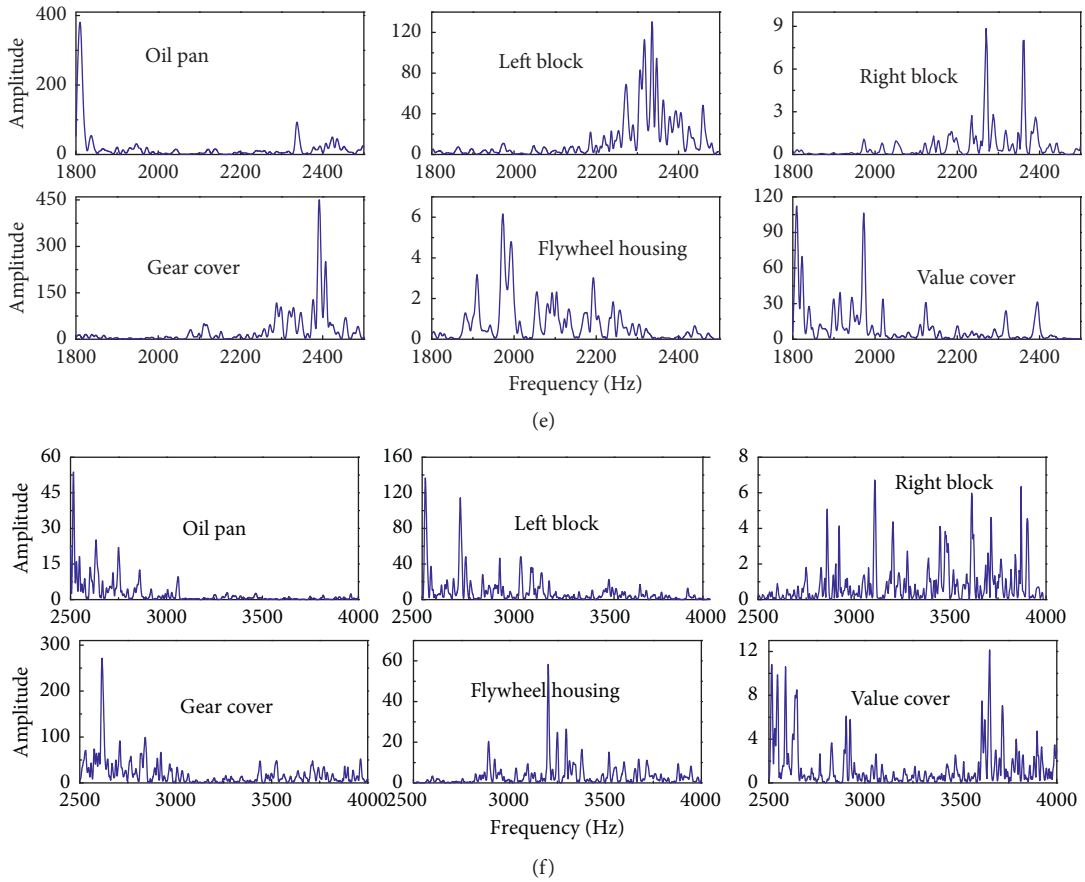

Figure 7: The input partial coherent power spectra of (a) 0–500 Hz, (b) 500–800 Hz, (c) 800–1200 Hz, (d) 1200–1800 Hz, (e) 1800–2500 Hz, and (f) 2500–4000 Hz.

The coherences of the component to the noise are (1) for 0–500 Hz, gear cover > oil pan > right block > left block- > flywheel housing > valve cover; (2) for 500–800 Hz, oil pan > valve cover > gear cover > flywheel housing > right block > left block; (3) for 800–1200 Hz, oil pan > left block- > gear cover > valve cover > flywheel housing > right block; (4) for 1200–1800 Hz, oil pan > gear cover > valve cover > left block > flywheel housing > right block; (5) for 1800–2500 Hz, gear cover > oil pan > left block > valve cover > right block- > flywheel housing; and (6) for 2500–4000 Hz, gear cover- > left block > flywheel housing > oil pan > valve cover > right block.

It can be seen that the input PCPS of the oil pan is the largest between a wide frequency band of 500–1800 Hz. It is because the lower vibration modes of such a thin-walled component are easy to excite due to the excitation of the body skirt. In other frequency bands, the gear cover shows the largest input PCPS below 500 Hz and above 1800 Hz. The main reasons are the resonances of the component in the low-frequency range and the dynamic meshing force between gear teeth at high frequency. So, the above two components are the top 2 contributors in most cases. For the left block, the amplitude of input PCPS in 1800–4000 Hz is considerable because the fuel injection pump and the air compressor radiate great portion of noise in this high-frequency range.

4.3. Weighting Analysis of Noise Sources

4.3.1. Analytic Hierarchy Tree. As analysed above, for a specific component (noise source), its contribution to the noise varies in different aspects, such as the frequency band, the testing point, and the engine speed. On this basis, the hierarchy tree (Figure 8) for weighting the noise sources consists of five levels from top to bottom: (1) objective level, (2) operating speed level, (3) testing point level, (4) frequency band level, and (5) noise sources level.

4.3.2. Fuzzy Consistency Matrix. The fuzzy consistency matrices for the frequency level are constructed according to the condition coherent power spectra and listed in Table 3. Based on the one-third octave SPL, the fuzzy consistency matrices for the test point level and the operating speed level can be calculated in the same way. Table 4 shows the fuzzy consistency matrix for the left testing point (C1). Table 5 presents the fuzzy consistency matrix for the engine speed of 1800 r/min (B3). For the top level, the fuzzy consistency matrix can be obtained based on the usage proportion of the engine speed and the A-weighted SPL, as shown in Table 6.

4.3.3. Weighting Order of Noise Sources. Based on the consistency matrices of adjacent levels, the combined weight

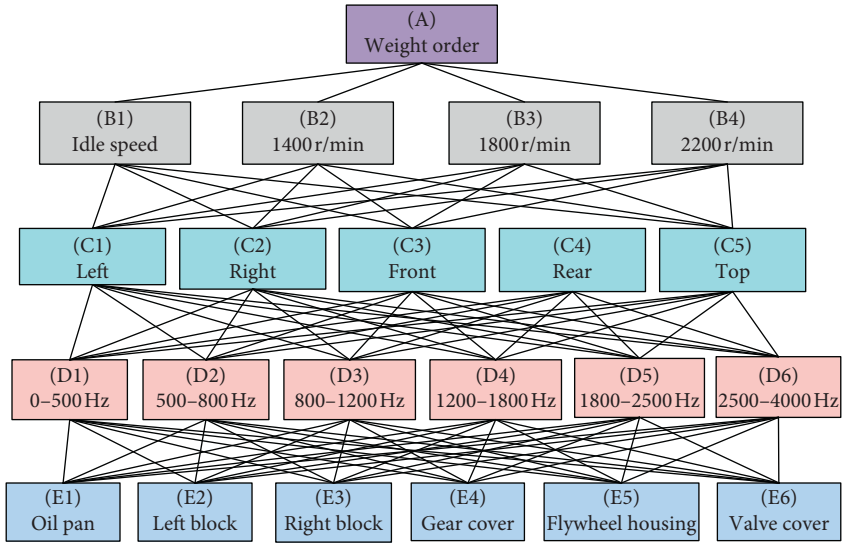

Figure 8: The hierarchy tree conducted for noise source weighting analysis.

Table 3: The fuzzy consistency matrices for the frequency level.

		E1	E2	E3	E4	E5	E6	Weight
D1 0–500 Hz	E1	0.500	0.630	0.638	0.466	0.647	0.659	0.229
	E2	0.370	0.500	0.508	0.336	0.517	0.529	0.134
	E3	0.362	0.492	0.500	0.328	0.508	0.521	0.129
	E4	0.534	0.664	0.672	0.500	0.681	0.693	0.265
	E5	0.363	0.483	0.492	0.319	0.500	0.512	0.125
	E6	0.341	0.471	0.479	0.307	0.488	0.500	0.118
D2 500–800 Hz	E1	0.500	0.728	0.695	0.662	0.676	0.587	0.286
	E2	0.272	0.500	0.467	0.433	0.447	0.359	0.110
	E3	0.305	0.533	0.500	0.467	0.481	0.393	0.126
	E4	0.338	0.567	0.533	0.500	0.514	0.426	0.145
	E5	0.324	0.553	0.519	0.486	0.500	0.412	0.137
	E6	0.413	0.641	0.607	0.574	0.588	0.500	0.197
D3 800–1200 Hz	E1	0.500	0.804	0.631	0.669	0.783	0.738	0.286
	E2	0.196	0.500	0.327	0.365	0.479	0.433	0.187
	E3	0.369	0.673	0.500	0.538	0.653	0.607	0.111
	E4	0.331	0.635	0.462	0.500	0.614	0.568	0.163
	E5	0.217	0.521	0.348	0.386	0.500	0.454	0.117
	E6	0.263	0.567	0.393	0.432	0.546	0.500	0.136
D4 1200–1800 Hz	E1	0.500	0.741	0.840	0.628	0.792	0.698	0.360
	E2	0.259	0.500	0.599	0.387	0.552	0.458	0.122
	E3	0.160	0.401	0.500	0.288	0.452	0.358	0.078
	E4	0.372	0.613	0.712	0.500	0.664	0.570	0.197
	E5	0.208	0.448	0.548	0.336	0.500	0.406	0.097
	E6	0.302	0.542	0.642	0.430	0.594	0.500	0.146
D5 1800–2500 Hz	E1	0.500	0.596	0.754	0.483	0.763	0.629	0.252
	E2	0.404	0.500	0.658	0.388	0.667	0.533	0.166
	E3	0.246	0.342	0.500	0.229	0.508	0.375	0.084
	E4	0.517	0.613	0.771	0.500	0.779	0.646	0.272
	E5	0.238	0.333	0.492	0.221	0.500	0.367	0.082
	E6	0.371	0.467	0.625	0.354	0.633	0.500	0.144
D6 2500–4000 Hz	E1	0.500	0.376	0.627	0.317	0.482	0.613	0.138
	E2	0.624	0.500	0.751	0.441	0.607	0.738	0.236
	E3	0.373	0.249	0.500	0.190	0.356	0.487	0.080
	E4	0.683	0.559	0.810	0.500	0.666	0.797	0.313
	E5	0.518	0.393	0.644	0.334	0.500	0.631	0.149
	E6	0.387	0.262	0.513	0.203	0.369	0.500	0.084

Table 4: The fuzzy consistency matrix for left testing point (C1) at 1800 r/min.

C1	D1	D2	D3	D4	D5	D6	Weight
D1	0.500	0.423	0.373	0.345	0.388	0.450	0.114
D2	0.577	0.500	0.450	0.422	0.464	0.527	0.157
D3	0.627	0.550	0.500	0.472	0.514	0.577	0.192
D4	0.655	0.578	0.528	0.500	0.543	0.605	0.215
D5	0.613	0.536	0.486	0.458	0.500	0.563	0.181
D6	0.550	0.473	0.423	0.395	0.438	0.500	0.141

Table 5: The fuzzy consistency matrix for engine speed of 1800 r/min (B3).

B3	C1	C2	C3	C4	C5	Weight
C1	0.500	0.624	0.577	0.638	0.661	0.293
C2	0.376	0.500	0.453	0.514	0.537	0.176
C3	0.423	0.547	0.500	0.561	0.584	0.213
C4	0.362	0.486	0.439	0.500	0.523	0.166
C5	0.339	0.463	0.416	0.477	0.500	0.152

Table 6: The fuzzy consistency matrix for target level (A).

A	B1	B2	B3	B4	Weight
B1	0.500	0.412	0.312	0.350	0.155
B2	0.588	0.500	0.400	0.437	0.222
B3	0.688	0.600	0.500	0.537	0.336
B4	0.650	0.563	0.463	0.500	0.287

matrices can be obtained. Table 7 gives the combined weight coefficients for the left testing point (C1), and Table 8 is the combined weight coefficients for 1800 r/min (B3). The contributions of the noise source to the radiated noise at different engine speeds are calculated and shown in Figure 9.

The contribution of the component to the overall noise changes with the engine speed. But some patterns still can be

Table 7: The combined weight matrix for the left testing point (C1).

C1-D-E	D1 0.114	D2 0.157	D3 0.192	D4 0.215	D5 0.181	D6 0.141	Weight
E1	0.229	0.286	0.286	0.360	0.252	0.138	0.268
E2	0.134	0.110	0.187	0.122	0.166	0.236	0.158
E3	0.129	0.126	0.111	0.078	0.084	0.080	0.099
E4	0.265	0.145	0.163	0.197	0.272	0.313	0.220
E5	0.125	0.137	0.117	0.097	0.082	0.149	0.115
E6	0.118	0.197	0.136	0.146	0.144	0.084	0.140

Table 8: The combined weight matrix for the engine speed of 1800 r/min (B3).

B3-C-D-E	C1 0.293	C2 0.176	C3 0.213	C4 0.166	C5 0.152	Weight
E1	0.268	0.259	0.259	0.263	0.266	0.263
E2	0.158	0.163	0.162	0.162	0.161	0.161
E3	0.099	0.104	0.105	0.103	0.102	0.102
E4	0.220	0.215	0.212	0.213	0.212	0.215
E5	0.115	0.119	0.120	0.118	0.117	0.118
E6	0.140	0.140	0.142	0.141	0.142	0.141

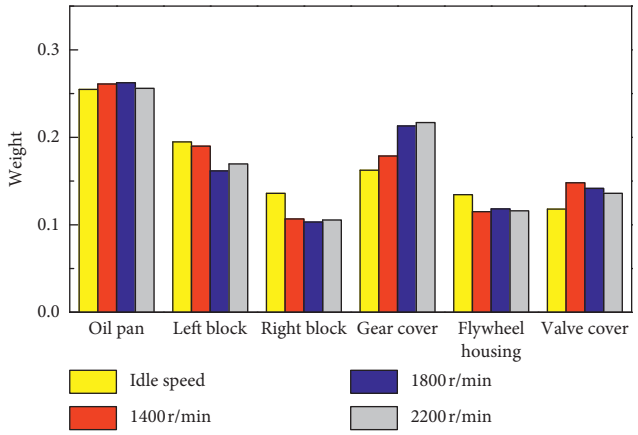

Figure 9: The weight of components at different speeds.

found. The oil pan is the most significant contributor regardless of engine speed, followed by the gear cover and the left block. At lower engine speeds, idle, and 1400 r/min, the contributions from gear cover and left block are quite close, while the gear cover contributes more at higher engine speeds (1800 r/min and 2200 r/min). The contributions of the right block, the flywheel, and the valve cover are similar and less important in this case.

4.3.4. Result Validation and Discussion. The overall weighting coefficients of the components to the radiated noise (Table 9) are calculated on the basis of the combined weight matrices considering the surface area effect. The surface area effect here relates to the outer surface of the component and acts by means of area factor. A component with the large outer surface is supposed to make greater contribution to the noise radiation comparing with a smaller one. Without considering the surface area effect, the weighting order of components is oil pan > gear cover > left block > valve cover > flywheel housing > right block. When the surface area is taken into account, the weighting order slightly changes into oil pan > left block > gear cover > valve cover > flywheel housing > right block.

Table 9: The final weight matrix of components to the overall noise.

A–E	B1	B2	B3	B4	Area factor	Overall weight	
	0.155	0.222	0.336	0.287		Without area effect	With area effect
E1	0.255	0.261	0.263	0.256	0.405	0.259	0.421
E2	0.195	0.19	0.161	0.17	0.196	0.176	0.138
E3	0.136	0.107	0.102	0.105	0.213	0.109	0.094
E4	0.162	0.179	0.215	0.217	0.162	0.199	0.129
E5	0.134	0.115	0.118	0.116	0.202	0.120	0.097
E6	0.118	0.148	0.141	0.136	0.221	0.137	0.121

Table 10: The tested near-field noise and the weighting order of components at 700 r/min.

Components	Near-field noise (dB)	Calculated weighting order
Oil pan left block	101.1	1
Left block	98.9	2
Right block	98.6	3
Gear cover	95.6	5
Flywheel housing	97.9	4
Valve cover	94.6	6

Table 11: The combined weight matrix of components for 0–500 Hz at 1800 r/min.

B3-D1-E	C1-D1 0.224	C2-D1 0.171	C3-D1 0.244	C4-D1 0.163	C5-D1 0.198	Weight
E1	0.229	0.247	0.243	0.246	0.238	0.240
E2	0.134	0.139	0.141	0.148	0.136	0.139
E3	0.129	0.124	0.121	0.115	0.126	0.123
E4	0.265	0.239	0.248	0.247	0.251	0.251
E5	0.125	0.127	0.119	0.115	0.128	0.123
E6	0.118	0.124	0.128	0.129	0.121	0.124

The calculated weighting order of the components to the overall noise is verified using the near-field noise in different operating conditions. The measured near-field noise of components and the computed weighting order under 700 r/min are given in Table 10 as an example. It can be seen from the comparison that the calculated weighting order of components are consistent with the near-field noise measurement. This clearly proves the validity of the proposed approach for noise source weighting of the diesel engine.

According to the overall weighting order, the main objective of the noise control of this diesel engine can be determined. But the detailed strategy still depends on the contributions from different aspects: engine speed and frequency band. Table 11 gives the weight coefficients of the engine component regarding the frequency range of 0–500 Hz at the engine speed of 1800 r/min. The calculated weighting orders of noise sources to the noise in different frequency bands at different speeds are given in Figure 10.

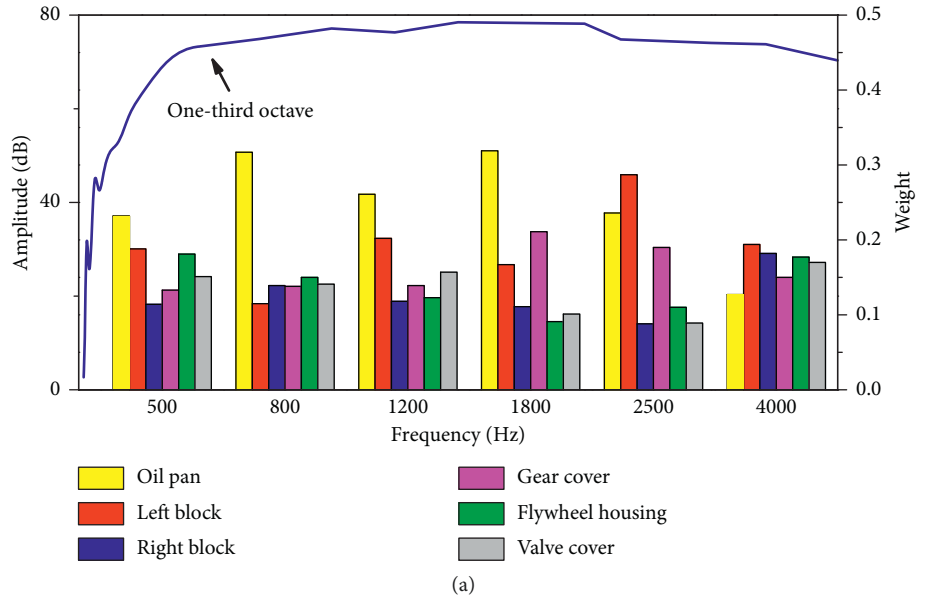

(a)

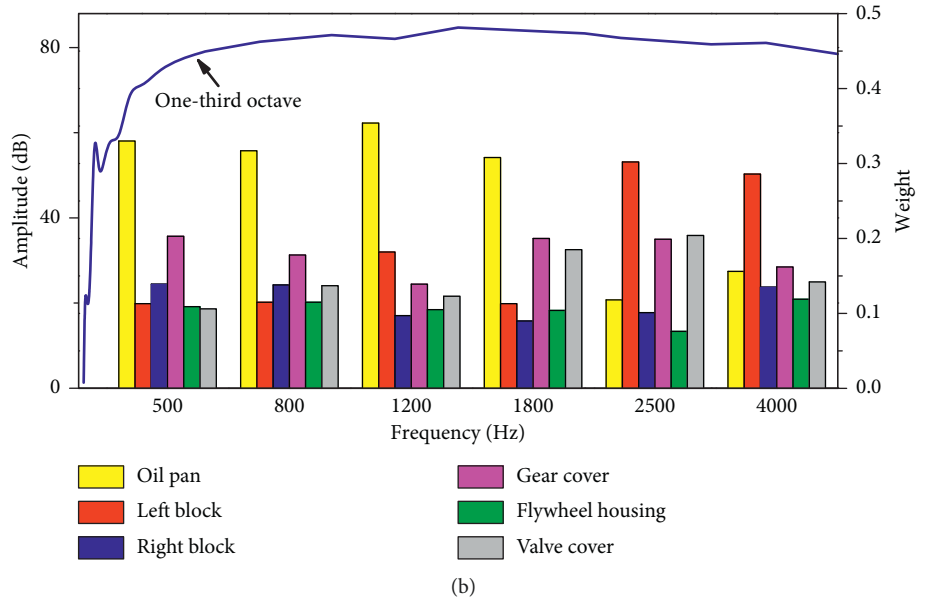

(b)

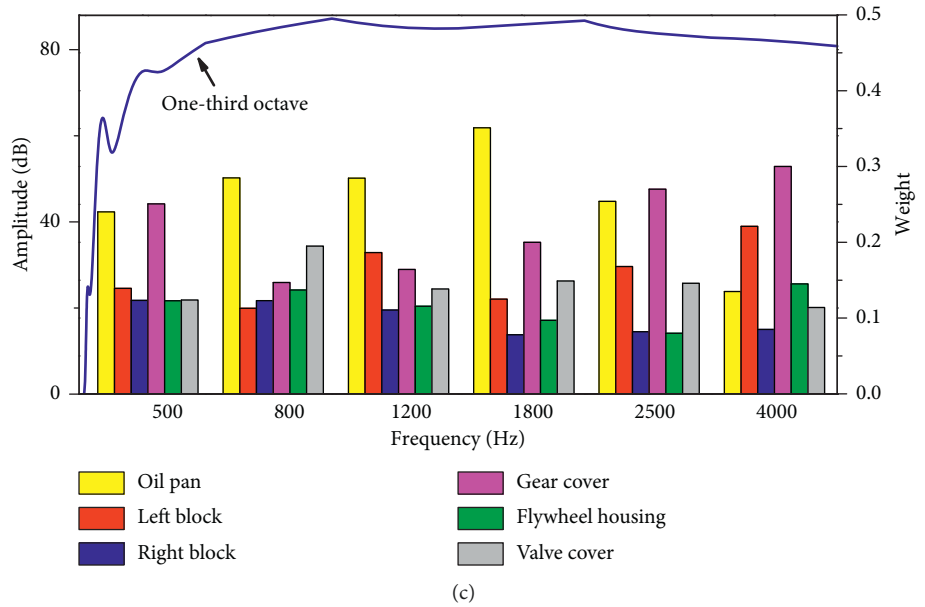

(c)

Figure 10: Continued.

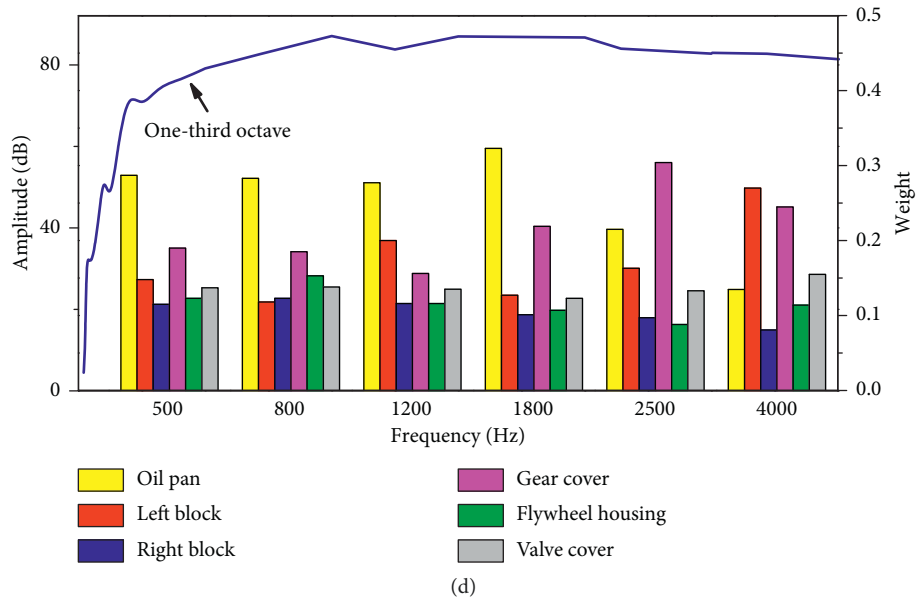

Figure 10: Contributions of the noise source to the noise in different frequency bands at (a) 700 r/min, (b) 1400 r/min, (c) 1800 r/min, and (d) 2200 r/min.

As discussed above, the contribution of components to the overall noise depends on the frequency band and the engine speed. For the radiated noise below 1800 Hz, the oil pan is almost the greatest contribution for all engine speeds considered. The oil pan even dominates over other components for some frequency bands at some speeds, e.g., 500–800 Hz at 700 r/min, 0–1800 Hz at 1400 r/min, and 500–1800 Hz at 1800 r/min. In the case of higher frequency noise, the left block contributes most at 700 r/min and 1400 r/min, and the gear cover takes the first place at higher speeds except for the case of 2500–4000 Hz at 2200 r/min.

The 1800 r/min case is the only exception that the gear cover breaks the dominance of the oil pan in the frequency range below 1800 Hz. At this speed, the weight of the gear cover is a little bit higher than the oil pan. It may be because the low-order vibration modes of the gear cover are excited up due to the rigid connection with the engine block. For the same reason, the flywheel housing also contributes considerably at idle speed (700 r/min).

The left block plays an important role in the frequency range higher than 1800 Hz. Since the right side of the engine block does not show a similar performance as the left side, the combustion excitation can be excluded from the reasons behind. It is noted that fuel injection pump and air compressor are rigidly mounted on the left block, which can radiate high-frequency noise.

Apart from the left block, the gear cover is even more noticeable in the frequency range of 1800 to 4000 Hz at 1800 r/min and 2200 r/min. At high speeds, the dynamic meshing force of gears becomes significant, and it can directly transmit to the gear cover through the transmission shaft. Therefore, a considerable radiated noise from this component can be found in the high-frequency range, e.g., 1800–2500 Hz and 2500–4000 Hz.

The radiated noise from the valve cover mainly relates to the combustion process and the valve movements. At lower speed, it is known the combustion excitation is more significant than the mechanical excitation. Although the noise due to valve movements is low at low speed, the valve cover still has important effect on the overall noise at 700 r/min and 1400 r/min. As the engine speed increases, the contribution of the valve cover decreases first and then rises again. It is because the high-speed movement of the valve parts starts to take the place.

5. Conclusions

An integrated approach of VMD-PCA-FAHP is proposed for noise source weighting of the diesel engine. Based on the noise and vibration measurement, the approach is implemented on the weighting analysis, and the result is validated using the near-field noise. Conclusions can be drawn as follows:

(1) The integrated VMD-PCA-FAHP approach is applicable in noise source identification and weighting analysis of the diesel engine. It can provide reliable weighting results in terms of contribution of engine component to noise.

(2) The VMD decomposes the noise signal into several meaningful IMFs, and the frequency bands can be determined by the time-frequency analysis. The correlations between component vibration and noise can be dig out by the PCA without coupled effect from other components.

(3) The FAHP eliminates the subjective influence of jury evaluation on the conduction of the consistency matrix. It also simplifies the process in searching the weighting matrix of high consistency.

(4) Considering the surface area effect, the overall weighting order of engine components to the radiated noise is oil pan > left block > gear cover > valve cover > flywheel housing > right block.

Data Availability

The data used to support the findings of this study are available from the corresponding author upon request.

Conflicts of Interest

The authors declare that they have no conflicts of interest.

Acknowledgments

The authors gratefully acknowledge the National Key R&D Program of China (2017YFC0211301).

References

[1] S. d'Ambrosio and A. Ferrari, "Diesel engines equipped with piezoelectric and solenoid injectors: hydraulic performance of the injectors and comparison of the emissions, noise and fuel consumption," *Applied Energy*, vol. 211, pp. 1324–1342, 2018.

[2] A. J. Torregrosa, A. Broatch, R. Novella et al., "Impact of gasoline and diesel blends on combustion noise and pollutant emissions in premixed charge compression ignition engines," *Energy*, vol. 137, pp. 58–68, 2017.

[3] H. Liu, J. Zhang, P. Guo, F. Bi, H. Yu, and G. Ni, "Sound quality prediction for engine-radiated noise," *Mechanical Systems and Signal Processing*, vol. 56-57, pp. 277–287, 2015.

[4] C. Serviere, J. L. Lacoume, and M.E Badaoui, "Separation of combustion noise and piston-slap in diesel engine, Part II: separation of combustion noise and piston-slap using blind source separation," *Mechanical Systems & Signal Processing*, vol. 19, no. 6, pp. 1218–1229, 2005.

[5] M.-H. Lu and M. U. Jen, "Source identification and reduction of engine noise," *Noise Control Engineering Journal*, vol. 58, no. 3, pp. 251–258, 2010.

[6] S. Brühl and A. Röder, "Acoustic noise source modelling based on microphone array measurements," *Journal of Sound and Vibration*, vol. 231, pp. 611–617, 2000.

[7] R. D. Sante and G. L. Rossi, "A new approach to the measurement of transverse vibration and acoustic radiation of automotive belts using laser Doppler vibrometry and acoustic intensity techniques," *Measurement Science and Technology*, vol. 12, pp. 525–533, 2001.

[8] M. E. Badaoui, J. Danière, F. Guillet, and C. Servière, "Separation of combustion noise and piston-slap in diesel engine-part I: separation of combustion noise and piston-slap in diesel engine by cyclic Wiener filtering," *Mechanical Systems and Signal Processing*, vol. 19, no. 6, pp. 1209–1217, 2005.

[9] M. Akil and C. Servière, "Separability of convolutive mixtures: application to the separation of combustion noise and piston-slap in diesel engine," in *Independent Component Analysis and Blind Signal Separation*, pp. 319–326, Springer, Berlin, Heidelberg, 2006.

[10] J. Wang, L. Tang, Y. Luo et al., "A weighted EMD-based prediction model based on TOPSIS and feed forward neural network for noised time series," *Knowledge-Based Systems*, vol. 132, pp. 167–178, 2017.

[11] Y. Zhang, J. Lian, and F. Liu, "An improved filtering method based on EEMD and wavelet-threshold for modal parameter identification of hydraulic structure," *Mechanical Systems and Signal Processing*, vol. 68-69, pp. 316–329, 2016.

[12] M. Buzzoni, E. Mucchi, and G. Dalpiaz, "A CWT-based methodology for piston slap experimental characterization," *Mechanical Systems and Signal Processing*, vol. 86, pp. 16–28, 2017.

[13] X. Liu and R. B. Randall, "Blind source separation of internal combustion engine piston slap from other measured vibration signals," *Mechanical Systems and Signal Processing*, vol. 19, no. 6, pp. 1196–1208, 2005.

[14] A. Albarbar, F. Gu, and A. D. Ball, "Diesel engine fuel injection monitoring using acoustic measurements and independent component analysis," *Measurement*, vol. 43, no. 10, pp. 1376–1386, 2010.

[15] W. Tao, T. Schuller, M. Huet, and F. Richecoeur, "Coherent entropy induced and acoustic noise separation in compact nozzles," *Journal of Sound and Vibration*, vol. 394, pp. 237–255, 2017.

[16] T. L. Saaty, "The analytic hierarchy process: planning, priority setting, resource allocation," in *The Analytic Hierarchy Process: Planning, Priority Setting, Resource Allocation*, McGraw-Hill, New York, NY, USA, 1980.

[17] T. L. Saaty, "How to make a decision: the analytic hierarchy process," *Interfaces*, vol. 24, no. 6, pp. 19–43, 1994.

[18] X. Liang, "Non-harmonic radiation noise source identification of engines based on the cepstrum analysis and analytic hierarchy process," in *Proceedings of SAE Technical Papers Series*, p. 4, Washington, DC, USA, May 2013.

[19] J. Zhang, J. Wang, J. Lin et al., "Diesel engine noise source identification based on EEMD, coherent power spectrum analysis and improved AHP," *Measurement Science & Technology*, vol. 26, no. 9, article 095010, 2015.

[20] H. Nezarat, F. Sereshki, and M. Ataei, "Ranking of geological risks in mechanized tunneling by using fuzzy analytical hierarchy process (FAHP)," *Tunnelling and Underground Space Technology*, vol. 50, pp. 358–364, 2015.

[21] J. Ooi, M. A. B. Promentilla, R. R. Tan et al., "Integration of fuzzy analytic hierarchy process into multi-objective computer aided molecular design," *Computers & Chemical Engineering*, vol. 109, 2018.

[22] H. J. Zimmermann, *Fuzzy Set Theory-and Its Applications*, Kluwer-Nijhoff Pub, Leiden, Netherlands, 1985.

[23] L. A. Zadeh, "Fuzzy sets," *Information and Control*, vol. 8, no. 3, pp. 338–353, 1965.

[24] Y. Min and S. Zhang, "Fuzzy consistent matrix and its application," *Journal of Systems Engineering & Electronics*, vol. 8, no. 1, pp. 57–64, 2012.

[25] L. W. Lee, *Group Decision Making with Incomplete Fuzzy Preference Relations Based on the Additive Consistency and the Order Consistency*, Pergamon Press Inc., Oxford, UK, 2012.

[26] S.-M. Chen, T.-E. Lin, and L.-W. Lee, "Group decision making using incomplete fuzzy preference relations based on the additive consistency and the order consistency," *Information Sciences*, vol. 259, no. 14, pp. 1–15, 2014.

[27] J. Krej, *On Additive Consistency of Interval Fuzzy Preference Relations*, Pergamon Press Inc., Oxford, UK, 2017.

[28] H. Zhou, M. Jia, Y. Feng et al., "Evaluation system for automatic fare gate capacity based on delphi and improved FAHP," in *Proceedings of Data Driven Control and Learning Systems Conference*, pp. 754–759, Chongqing, China, May 2017.

[29] J.-P. Gao, Z.-S. Xu, D.-L. Liu, and H.-H. Cao, "Application of the model based on fuzzy consistent matrix and AHP in the assessment of fire risk of subway tunnel," *Procedia Engineering*, vol. 71, no. 16, pp. 591–596, 2014.

[30] K. Dragomiretskiy and D. Zosso, "Variational mode decomposition," *IEEE Transactions on Signal Processing*, vol. 62, no. 3, pp. 531–544, 2014.

[31] P. Dey, U. Satija, and B. Ramkumar, "Single channel blind source separation based on variational mode decomposition and PCA," in *Proceedings of 2015 Annual IEEE India Conference (INDICON)*, pp. 1–5, New Delhi, India, December 2015.

[32] G. Shu and X. Liang, "Identification of complex diesel engine noise sources based on coherent power spectrum analysis," *Mechanical Systems and Signal Processing*, vol. 21, no. 1, pp. 405–416, 2007.

[33] H. B. Huang, X. R. Huang, M. L. Yang, T. C. Lim, and W. P. Ding, "Identification of vehicle interior noise sources based on wavelet transform and partial coherence analysis," *Mechanical Systems and Signal Processing*, vol. 109, pp. 247–267, 2018.

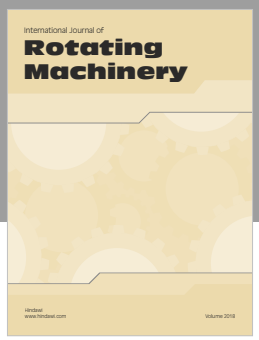

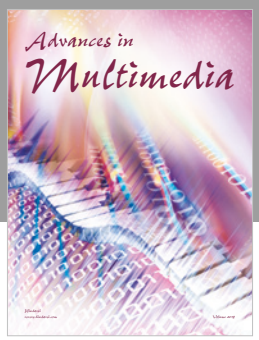

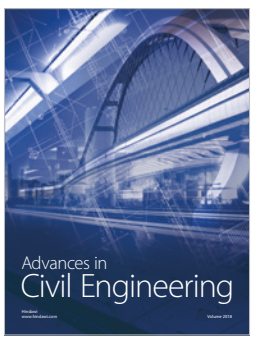

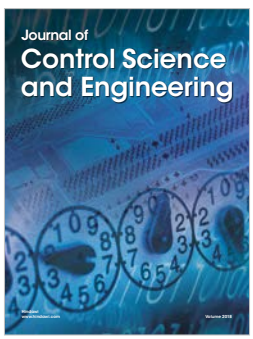

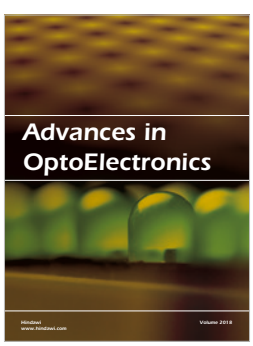

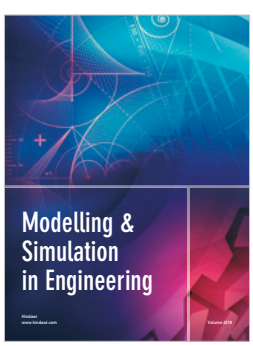

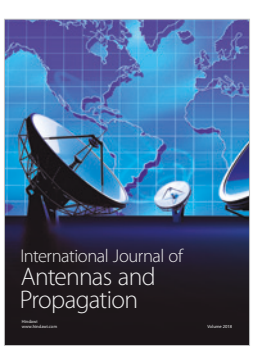

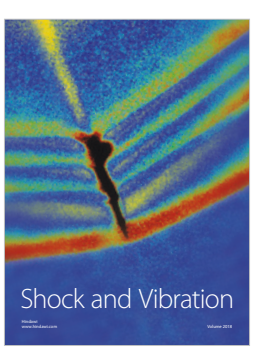

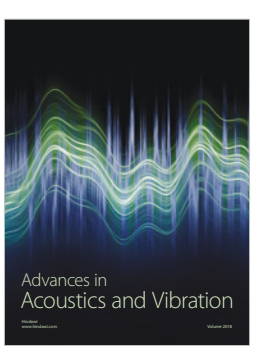

Hindawi

Submit your manuscripts at
www.hindawi.com